processes

MDPI

Article

Multi-Scale Characterization of Reservoir Space Features in Yueman Area of Fuman Oilfield in Tarim Basin

Yintao Zhang [1,2], Chengyan Lin [1], Lihua Ren [1], Chong Sun [2], Jing Li [3,*], Xingyu Zhao [3] and Mingyang Wu [3]

[1] School of Geosciences, China University of Petroleum (East China), Qingdao 266580, China
[2] Research and Development Center for Ultra-Deep Complex Reservoir Exploration and Development, China National Petroleum Corporation, Korla 841000, China
[3] State Key Laboratory of Deep Oil and Gas, China University of Petroleum (East China), Qingdao 266580, China; mingyangwu002@163.com (M.W.)
* Correspondence: lijingupc2022@163.com

Abstract: Reservoir space characteristics are the key to reservoir evaluation and the evaluation of reservoir capacity. The reservoir space of fracture-vuggy carbonate reservoirs is complex and diverse, and it develops from micro to macro. There is a lack of systematic study on the reservoir space of the Ordovician fracture-vuggy carbonate reservoir. Therefore, taking the Ordovician Yijianfang Formation in Yueman Block of Fuman Oilfield in Tarim Basin as an example, the microscopic reservoir space characteristics of the study area were characterized by rock thin section identification, X-ray diffraction, scanning electron microscopy, high-pressure mercury injection, and low-temperature nitrogen adsorption experiments, and the macroscopic reservoir space characteristics of the study area were characterized by core observation, drilling and logging data, and imaging logging data. The results showed that (1) the lithology of the Ordovician Yijianfang Formation in the Yueman area of Fuman Oilfield is mainly micrite and sparry grain limestone. The mineral composition is mainly calcite, accounting for 97.35%, containing a small amount of quartz and dolomite, accounting for 1.1% and 1.55%, respectively. (2) At the micro level, the reservoir space of Yijianfang Formation in Yueman Block is not developed in primary pores, mainly having developed dissolution pores, structural fractures, and pressure solution fractures, and the pore size is distributed from the nanometer to micron scale. (3) The dissolution caves in the study area are developed at the macro level, mainly including pore-type, cave-type, fracture-pore-type, and fracture-type reservoirs. The research results provide technical support for the accurate evaluation of fractured-vuggy carbonate reservoirs and the improvement of exploration and development effects.

Keywords: fractured vuggy reservoir; reservoir space; carbonate rock; Yueman Formation; Tarim Basin

Academic Editor: Qingbang Meng

Received: 11 December 2024
Revised: 31 December 2024
Accepted: 13 January 2025
Published: 23 January 2025

Citation: Zhang, Y.; Lin, C.; Ren, L.; Sun, C.; Li, J.; Zhao, X.; Wu, M. Multi-Scale Characterization of Reservoir Space Features in Yueman Area of Fuman Oilfield in Tarim Basin. *Processes* **2025**, *13*, 310. https://doi.org/10.3390/pr13020310

1. Introduction

Fractured-vuggy carbonate reservoirs are rich in resources and have become an important new field for increasing oil and gas reserves and production [1,2]. The accurate characterization of reservoir space is the key to effectively evaluating the reservoir capacity and fluid migration of oil and gas reservoirs [3–5]. Many scholars at home and abroad have carried out research on the characteristics of carbonate reservoir space. Zheng [6] et al. and Bao [7] et al. studied the types of reservoir space by observing casting thin sections, fluorescent thin sections, and scanning electron microscopy; On the basis of core, thin section, logging data, imaging logging data, and field outcrop analysis, Ren [8] et al.

systematically studied the microfacies types and reservoir space characteristics of the Ordovician Yingshan Formation. Based on core observations, thin section identification, and scanning electron microscope imaging, Ren et al. [9] used FIB-SEM three-dimensional imaging technology to analyze the characteristics of carbonate reservoirs in the Middle Permian Maokou Formation in southern Sichuan. Based on core descriptions, thin section identification, physical property analysis, comprehensive mud logging, and reservoir prediction, Liu Jun et al. [10] characterized the middle and lower Ordovician reservoirs in the Shunnan area of Tarim Basin. Huang Wenhui et al. [11] divided the reservoir space types on the basis of field geological observation, core observation and analysis, and conventional thin section and cast thin section observation and identification and made a preliminary analysis on the formation and evolution of different reservoir spaces. Lin et al. [12] used rock thin sections, whole rock X-ray diffraction, nuclear magnetic resonance, and scanning electron microscopy to study the reservoir space, pore structure, and oil-bearing properties of different lithofacies reservoirs. However, the reservoir space of fractured and vuggy carbonate reservoirs is extremely complex, with pores, caverns, and fractures developing at scales ranging from micro and nano to meter; and with strong heterogeneity and anisotropy, the study of reservoir space using a single method has limitations and inaccuracy [13,14].

Fuman Oilfield in the Tarim Basin has formed a large-scale marine fractured-vuggy carbonate reservoir after multi-stage cyclic tectonic evolution. The reservoir space is complex and diverse, and the pores are developed from micro to macro [15–17]. However, the multi-scale characterization of reservoir space characteristics in Fuman Oilfield is rarely reported. Therefore, on the basis of rock thin section identification and X-ray diffraction whole rock analysis, the whole pore size distribution of the microscopic reservoir space is characterized by high-pressure mercury injection and low-temperature nitrogen adsorption. Combined with core observations, drilling and logging data, and imaging logging data, the micro–macro system of fracture-cavity carbonate reservoir space was studied.

2. Condition of the Study Area

2.1. Regional Geological Conditions

The Yueman area of Fuman Oilfield in Tarim Basin is located in the transitional part between the northern depression and the Tabei uplift in the seven first-order tectonic units of the three uplifts and four depressions in Tarim Basin, Xinjiang Uygur Autonomous Region [18]. Its main body is located in the Aman transition zone of the second-order tectonic unit in the northern depression, and the overall structure is gentle, showing a southwest dip slope. The northeast and northwest strike-slip faults are developed and characterized by multi-stage extrusion deformation, early formation, and early setting. Multi-stage tectonic activities and late karst superposition led to the development of fractures and caves in the study area, which were longitudinally banded or beaded and had strong heterogeneity [19–21] (Figure 1).

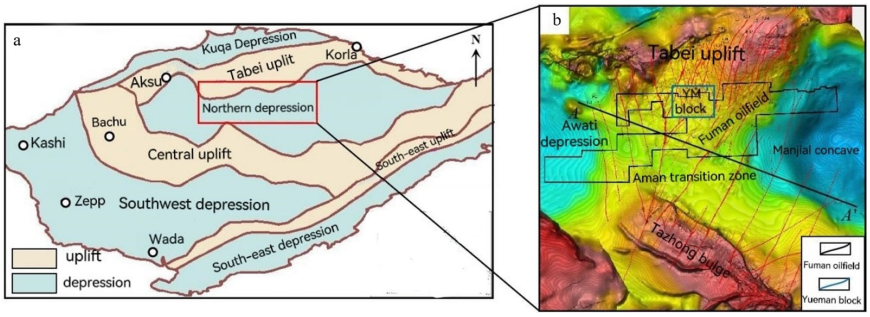

Figure 1. Location and structure map of study area (modified from Tarim Oilfield): (**a**) study area location, (**b**) study area structure map.

2.2. Formation Development Characteristics

The transitional zone of Aman-man in Tarim Basin is well developed, and drilling reveals that it developed from the Cenozoic to the Paleozoic. The Ordovician Yijianfang Formation and Yingshan Formation are the main exploration horizons, and large-scale fracture-cavity carbonate reservoirs are developed [22–24]. The development of Ordovician strata in the study area is relatively complete (Table 1) [25].

Table 1. Ordovician stratigraphic division in Yueman Block.

System	Series	Stratum Formation	Member	Stratigraphic Code Contact Relationship	Lithological Characteristics
O	O_3	Tierekeawati Formation	-	O_3tr	Silt sandstone, fine sandstone, mudstone
		Sangtamu Formation	Clastic rock member	O_3s	Interbedding of calcareous mudstone and argillaceous limestone
		Lianglitage Formation	Nodular limestone Member	O_3l	Mud crystal limestone, nodular limestone, algal binding rock
		Tumuxiuke Formation	Mudstone member	O_3t	Brown ash, brown micritic limestone, marl-bearing limestone
	O_2	Yijianfang Formation	-	O_2y	Sand-gravel limestone Burmese limestone
	O_1	Yingshan Formation	Y1 member	$O_{1\text{-}2}y^1$	Mud-silt crystal limestone, calcarenite limestone
			Y2 member	$O_{1\text{-}2}y^2$	Sandy limestone, mud-powder crystal limestone

The five large strike-slip faults developed in the study area have been fractured to the main source rocks of the Lower Cambrian Yuertusi Formation in the vertical direction (Figure 2). The overlying Tumuxiuke Formation and Sangtamu Formation mudstones in Yueman Block have a thickness of 17~20 m and 580~670 m, respectively, which play a good sealing role and are high-quality regional cap rocks [26–28]. The oil and gas accumulation model of vertical migration, self-storage, and self-covering has laid a useful oil and gas accumulation condition for the formation of large oil and gas fields.

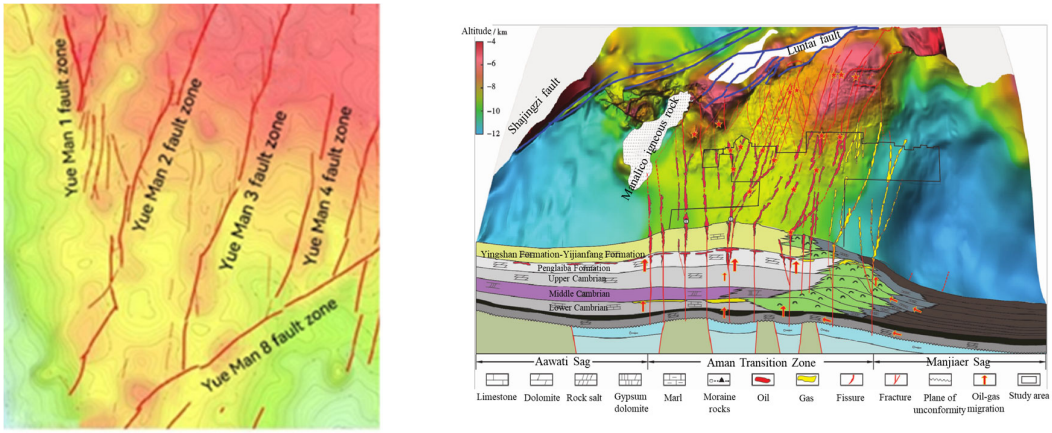

(**a**) (**b**)

Figure 2. Yueman Block fracture distribution map (modified from Tarim Oilfield): (**a**) spatial distribution, (**b**) stereoscopic distribution.

3. Sample Collection and Methods

3.1. Experimental Sample

In this study, based on the observation of drilling coring rock samples, 73 groups of rock thin sections of Yijianfang Formation in Yueman Block were selected. The well location distribution in the study area is shown in Figure 3, and four groups (M-1 well, 7272.5 m; M-2 well, 7216 m; M-5 well, 7270.2 m; M-8 well, 7209 m) were selected for core observation and thin section identification analysis.

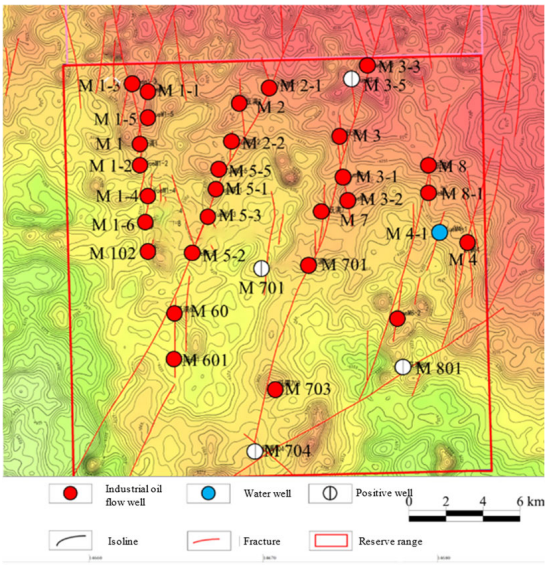

Figure 3. Yueman Block well location distribution map.

On the basis of core observation and thin section identification analysis, four groups of rock samples, Sample 1 (M-2 well, 7200.59 m), Sample 2 (M-5 well, 7265.73 m), Sample 3 (M-5 well, 7263.68 m), and Sample 4 (M-6 well, 7308.92 m), were selected for an X-ray diffraction whole rock experiment, high-pressure mercury injection experiment, and low-temperature nitrogen adsorption experiment.

3.2. Experimental Instruments and Methods

(1) Characterization method of reservoir petrological characteristics

Petrological characteristics are the basic physical characteristics of reservoirs. Different petrological characteristics will not only cause great differences in the microscopic characteristics of rocks, but will also cause great differences in their mechanical properties and seepage characteristics. Therefore, the microscopic pore structure characteristics of rocks are characterized by scanning electron microscopy and microscopic slices. The experimental instruments are shown in Figure 4.

(**a**) (**b**)

Figure 4. Experimental instruments: (**a**) field emission/focused ion beam scanning electron microscope; (**b**) laser scanning confocal microscope.

(2) Characterization method of reservoir petrological characteristics

On the basis of a large number of experiments, the effective range of pore size measured by mercury injection test to be greater than 50 nm. In order to accurately test the samples with a larger pore size, the AutoPore IV 9620 automatic high-performance mercury injection instrument of American Mac company in Norcross, Georgia, United States was used to test the pore size of rock samples. As shown in Figure 5, the test pressure range is 0.2~60,000 Psi, and the test pore size range is 3 nm~800 μm [29]. In the higher-pressure section, the matrix compression effect will be produced, which has a significant impact on the mesopores and micropores, resulting in an inaccurate pore diameter distribution of micropores and mesopores in the mercury intrusion test results. The high-pressure mercury intrusion method is more accurate for the measurement of pore diameters greater than 50 nm [30,31].

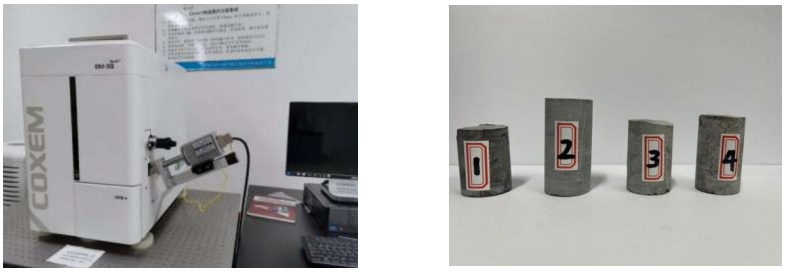

(**a**) (**b**)

Figure 5. High-pressure mercury injection experimental instruments and samples: (**a**) high-pressure mercury porosimeter; (**b**) high-pressure mercury intrusion samples.

(3) Low-temperature nitrogen adsorption test experiment

In order to accurately test samples with a small range of pore size (such as less than a 50 nm pore size), at the same time, the Tristar II 3020 automatic specific surface area physical adsorption instrument produced by Michael Company in Norcross, Georgia, United States was used to test the pore size of the rock samples. As shown in Figure 6, the measured rock pore size range is 0.35~500 nm. The test sample is the same as in the high-pressure mercury injection experiment (as shown in Figure 5b).

Figure 6. Low-temperature nitrogen adsorption experimental instrument.

Combined with the high-pressure mercury intrusion experiment and low-temperature nitrogen adsorption experiment, the full pore size distribution of rock samples in the study area was comprehensively characterized, as shown in Figure 7.

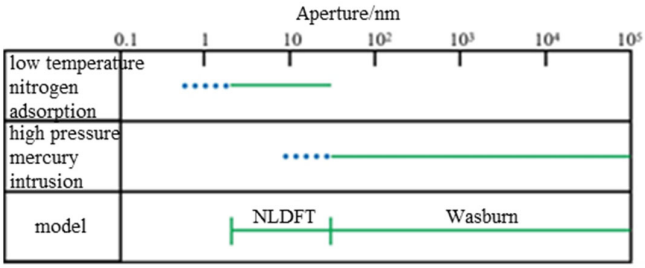

Figure 7. Joint characterization method and computational model.

4. Results and Discussion

4.1. Reservoir Petrology Characteristics

Petrological characteristics are the basic petrophysical characteristics of a reservoir [32–34]. The lithology of carbonate reservoirs in the study area is mainly limestone, with many soluble mineral components such as calcite. In the atmospheric water and burial environment, acidic fluid can dissolve soluble minerals such as calcite and provide secondary pores for reservoirs. Compared with sandstone and clastic rocks at the same depth, the pores are more developed and the permeability is higher. Due to the lower mineral composition, such as quartz in limestone, the compressive strength of rock is much smaller than that of sandstone. Therefore, through rock thin section identification and X-ray diffraction whole rock analysis, the petrological characteristics of the Yijianfang Formation reservoir in the study area are further deepened.

4.1.1. Reservoir Lithology Characteristics

Some rock samples and casting thin sections are shown in Figure 8, and lithology statistics are shown in Figure 9. The staining part of the figure is calcium violet staining to distinguish dolomite from calcite. It is found that the reservoir lithology of Yijianfang Formation in Yueman Block is mainly micrite and sparry grain limestone, which is mainly sparry bioclastic algal calcarenite, sparry algal mass bioclastic limestone, sparry algal calcarenite, sparry-argillaceous bioclastic limestone, micrite acetoclastic algal calcarenite, and bioclastic micrite limestone.

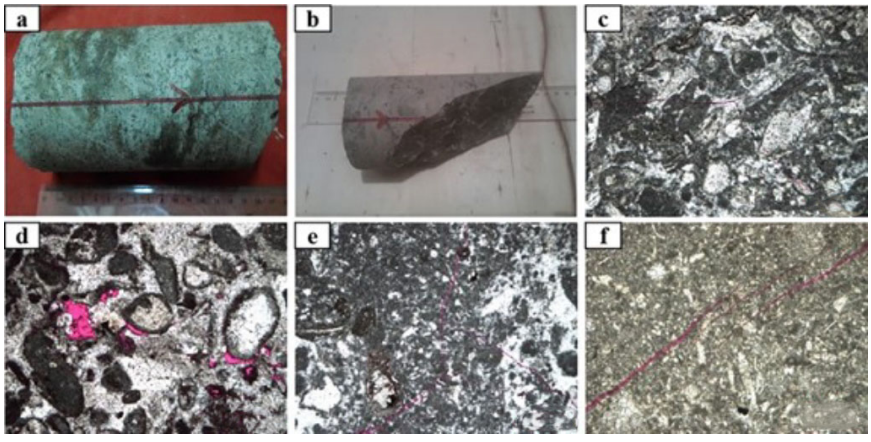

Figure 8. Core and cast thin section of Yijianfang Formation in Yueman Block (Tarim Oilfield Research Institute): (**a**) gray oily limestone, M-2 well, Yijianfang Formation, homing well section: 7215.88~216.03 m; (**b**) gray fluorescent limestone, M-5 well, Yijianfang Formation, homing well section: 7275.22~7275.28 m; (**c**) sparry bioclastic algal calcarenite, M-1 well, Yijianfang Formation, 7272.5 m; (**d**) sparry algal mass bioclastic limestone, M-2 well, Yijianfang Formation, 7216 m; (**e**) mud-bright crystal grain limestone, M-5 well, Yijianfang Formation, 7270.2m; (**f**) bioclastic micrite limestone, M-8 well, Yijianfang Formation, 7209 m.

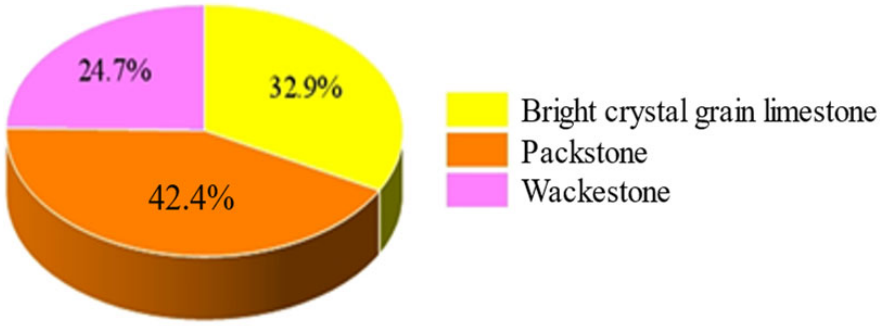

Figure 9. Lithology statistics of Yijianfang Formation in Yueman Block (from Tarim Oilfield).

4.1.2. Reservoir Mineral Content

The whole rock X-ray diffraction was carried out to quantitatively analyze the rock mineral composition of the reservoir in the study area. It can be seen from Figure 10b that the mineral species of Yijianfang Formation in Yueman Block are relatively few, being mainly calcite, and the average content of calcite is 97.35%. It contains a small amount of quartz and dolomite, with an average content of 1.1% and 1.55%, respectively. The content of calcite and quartz brittle minerals is high, and the reservoir has obvious brittleness and a strong fracturing ability. The soluble minerals of calcite and dolomite account for a large proportion, which lays a good material foundation for dissolution.

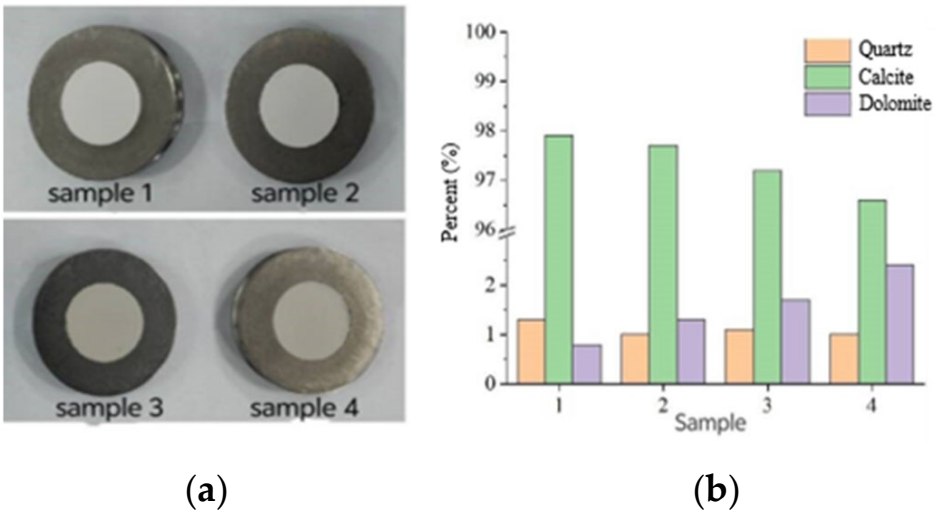

Figure 10. Experimental samples and experimental results: (**a**) XRD experimental samples, (**b**) mineral composition and proportion.

4.2. Characteristics of Micro–Macro Reservoir Space

The marine carbonate reservoirs of the Ordovician Yijianfang Formation in Yueman Block have formed fractured-vuggy carbonate rocks with a complex reservoir space through multi-stage tectonic and karst processes. The types of reservoir space mainly include pores, holes, and fractures (Table 2). Through casting thin sections, scanning electron microscopy, nitrogen adsorption, high-pressure mercury injection experiments, and imaging logging data, it is considered that Yijianfang Formation in Yueman Block is mainly divided into four types: cave reservoir, fracture-cavity reservoir, fracture reservoir, and cavity reservoir.

Table 2. Classification of Ordovician carbonate reservoir space.

Reservoir Space	Category		Scale (Diameter or Opening)/μm	Cause
Matrix pore	Intergranular dissolved pore		$<2 \times 10^3$	Diagenesis, fabric dissolution
	Dissolved pores in grains		0.1×10^2~1×10^3	
	Intercrystalline pore		0.1×10^2~2×10^2	
Cavern	Dissolution cave	Small cave	2×10^3~5×10^3	Non-fabric dissolution
		Medium cave	5×10^3~1×10^4	
		Big cave	1×10^4~1×10^5	
	Dissolution hole	Large hole	$>100 \times 10^3$	
Fracture	Structural fracture	Micro fracture	<10	Tectogenesis
		Small fracture	10~100	
		Medium fracture	100~1000	
		Large fracture	>1000	
	Compression fracture		1~100	Diagenesis
	Contraction fracture		1~100	
	Dissolution fracture		1~1000	Dissolution

4.2.1. Characteristics of Microscopic Reservoir Space

(1) High-pressure mercury intrusion test result

The mercury entry–exit curves of the four groups of samples are shown in Figure 8a. The mercury entry–exit curves of the samples and the pore structure characteristics of the mercury intrusion test are shown in Table 3. It can be seen from Table 3 that the displacement pressure of Samples No. 1–4 is 0.04 MPa, 0.02 MPa, 0.06 MPa, and 0.02 MPa, respectively, and the average displacement pressure is 0.035 MPa. The displacement pressure is low, and there are cracks and large pores, so oil and gas are easy to charge. The porosity is 2.62%, 2.59%, 2.85%, and 3.05%, respectively, and the average porosity is 2.78%. The mercury entry–removal curves of the four groups of samples are similar. From the mercury entry curve, the maximum mercury entry saturation of the samples is 66.75%, 64.92%, 76.67%, and 88.06%, respectively, and the average value of the maximum mercury intrusion saturation is 74.1%, reflecting that the pores in Yueman Block are more developed. In the low-pressure stage (<0.1 MPa), with the increase in the mercury injection pressure, the amount of mercury injection also increased, and the accumulation of mercury injection was high, indicating that there were a lot of open macropores larger than 100 microns in the sample. In the high-pressure stage (>10 MPa), with the increase in mercury pressure, the amount of mercury intake also increased, indicating that there were nano-scale pores in Samples 2 and 4, and the cumulative amount of mercury intake in Sample 4 was greater, indicating that there were more nano-scale pores in Sample 4.

Table 3. Experimental parameters of high-pressure mercury injection in Yueman Block.

Numbering	Rock Density ($cm^3 \cdot g^{-1}$)	Porosity (%)	Mercury Injection Saturation (%)	Specific Surface Area ($m^2 \cdot g^{-1}$)	Displacement Pressure (MPa)
1	2.61	2.62	66.75	0.302	0.04
2	2.56	2.59	64.92	0.156	0.02
3	2.73	2.85	76.67	0.279	0.06
4	2.98	3.05	88.06	0.337	0.02

From the mercury removal efficiency of the four groups of samples, it can be seen that the mercury removal rate is zero when the pressure is reduced to 0.1 MPa. The main reasons

for the analysis are as follows: First, when the mercury removal pressure is reduced to 0.1 MPa, the capillary pressure generated by all pores in the sample is less than the mercury removal pressure at this time, and the mercury solution cannot be removed. In the process of mercury injection, the capillary pressure is the resistance. When the external pressure exceeds the capillary pressure generated at throat A, the mercury flows into pore B due to the pressure difference. Because the pore B has a large pore size, the capillary pressure generated is much smaller than the external pressure. The liquid mercury enters the throat C port with a smaller pore size, the throat C radius is very small, the capillary pressure generated is much larger than the external pressure, and the liquid mercury cannot break through the pore C. With the gradual increase in external pressure, the liquid mercury can break through throat C and enter the pore connected at the other end of pore C. In the process of mercury removal, capillary pressure is the driving force. Only when the external pressure is reduced to less than the capillary pressure can the liquid mercury be removed from the throat; otherwise, the liquid mercury remains in the pores (Figure 11a). However, when comparing with the literature [35], the high-pressure mercury intrusion experiment in the literature shows that the samples used have nano-and micron-sized pores, but when the mercury removal pressure drops to 0.1 MPa, a certain amount of liquid mercury is also removed from the sample. Therefore, this reason is not the main reason for the mercury removal rate of the sample high-pressure mercury injection experiment to be zero when the pressure is reduced to 0.1 MPa. Second, in order to facilitate the analysis, it is assumed that throat A is completely closed and has a limited state. When the external pressure is greater than a certain pressure value, throat A opens, and the capillary pressure in throat A becomes lower than the external pressure, and the liquid mercury enters pore B under the action of the pressure difference (Figure 11b). When mercury is injected when the pressure reaches this critical value, the throat opens and the liquid mercury enters the pores. When the pressure is less than this value, the throat is closed again, and the liquid mercury in the pores cannot be removed, resulting in a large amount of mercury remaining in the pores. Considering that the sample comes from 7000 m deep, cracks will be generated under compaction during diagenesis, and it will also become denser. Therefore, it is speculated that this is the main reason why the mercury removal rate is zero when the pressure is reduced to 0.1 MPa.

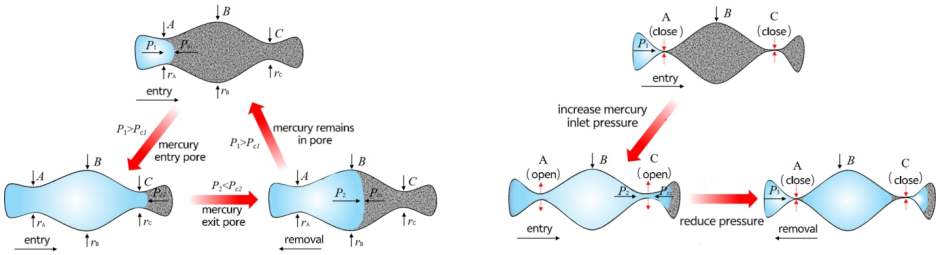

Figure 11. Mercury intake and removal diagram: (**a**) The first mercury entry–removal diagram, (**b**) the second mercury entry–removal diagram.

The pore size distribution curve of high-pressure mercury injection (Figure 12) shows that the pore size distribution of the Yijianfang group in Yueman Block is relatively wide, the pores above 10 nm are distributed, and the pore sorting is poor. The pore size distribution is mainly bimodal, and the pore size of the main peak is mainly between 100 and 150 μm. Combined with the mercury removal curve, many closed pores exist between 10 nm and 100 μm.

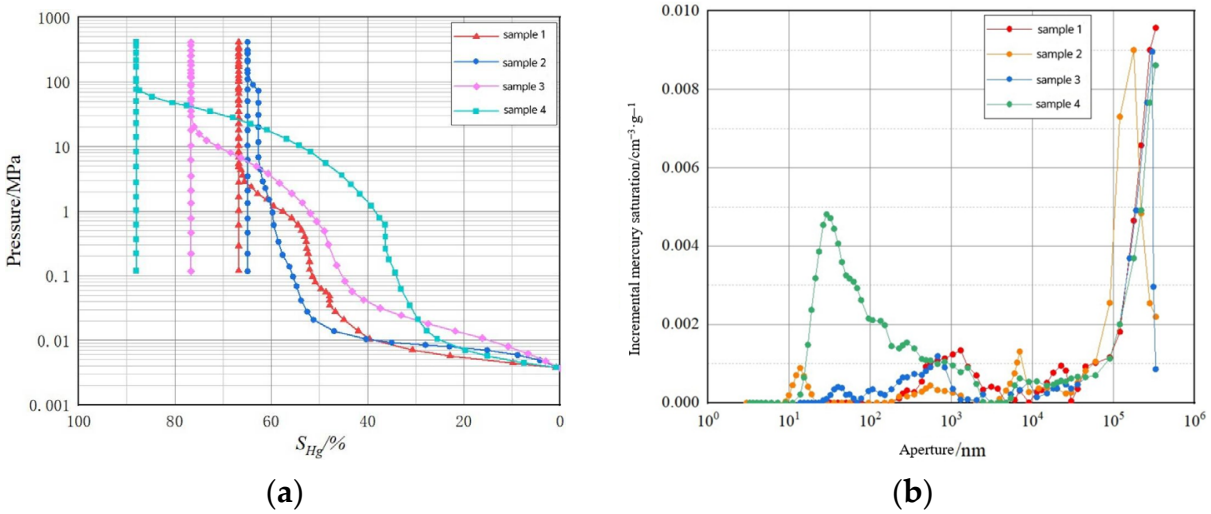

Figure 12. Experimental results of high-pressure mercury injection in Yueman Block: (**a**) mercury entry–removal curve, (**b**) pore size distribution.

(2) Low-temperature nitrogen adsorption test result

According to the characteristics of the hysteresis loop curve of low-temperature nitrogen adsorption, the IUPAC (International Union of Theoretical and Applied Chemistry, Triangle Park, NC, USA) divides the hysteresis loop into H1~H4 types (Figure 13), in which different types of hysteresis loop curves represent different microscopic pore morphology [36,37].

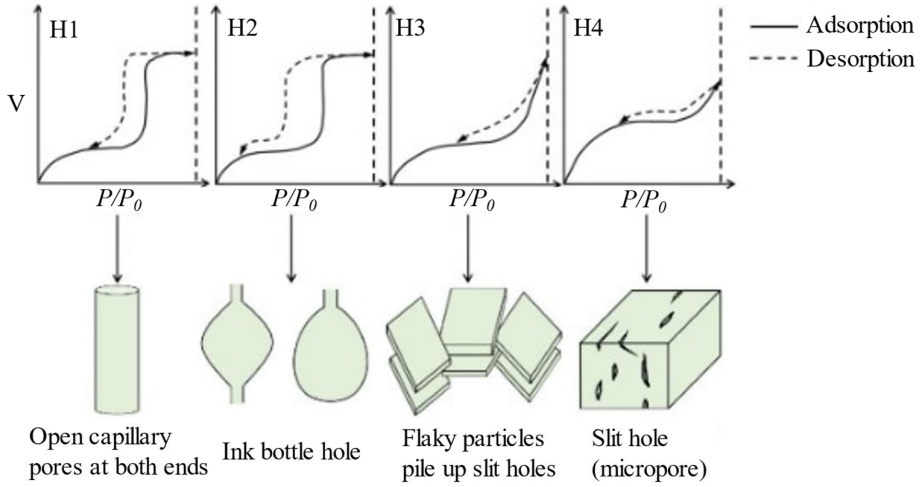

Figure 13. Classification of adsorption–desorption hysteresis rings.

According to the IUPAC (Triangle Park, NC, USA) recommended classification, the adsorption–desorption curve of Yijianfang Formation in Yueman Block (Figure 14a) is dominated by H3, with the characteristics of H2 and H4. It is shown that there are mainly three kinds of pore morphology: ink bottle pore, flake pore, and slit pore.

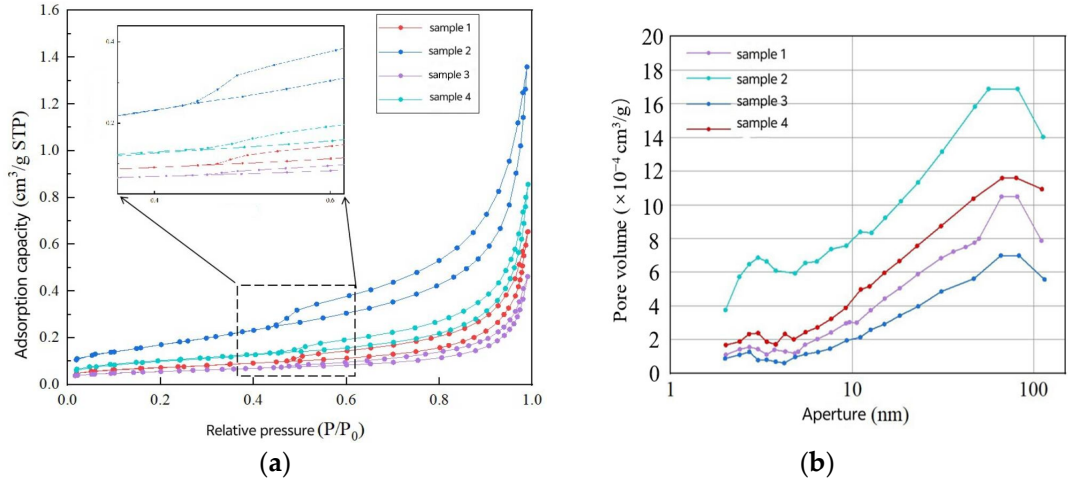

Figure 14. Experimental results of low-temperature nitrogen adsorption in Yueman Block: (**a**) adsorption–desorption curve, (**b**) pore size distribution.

The pore size distribution measured by low-temperature nitrogen adsorption is shown in Figure 14b. The pore volume of the sample increases with the pore size increase, and the pore size of the nitrogen adsorption test is mostly distributed between 10 and 100 nm. The pore distribution curve of the sample is mainly bimodal. The pore size of the main peak is mainly concentrated between 60 and 80 nm, and the pore size of the left peak is mainly concentrated between 4 and 6 nm.

(3) Joint characterization of full aperture volume distribution

The high-pressure mercury intrusion–nitrogen adsorption method was used to characterize the total pore size distribution of the matrix pores of Yijianfang Formation in Yueman Block (Figure 15). It was found that the matrix pores of Yijianfang Formation in Yueman Block were widely distributed, ranging from nanometer to micron, mainly large pores, and with poor sorting.

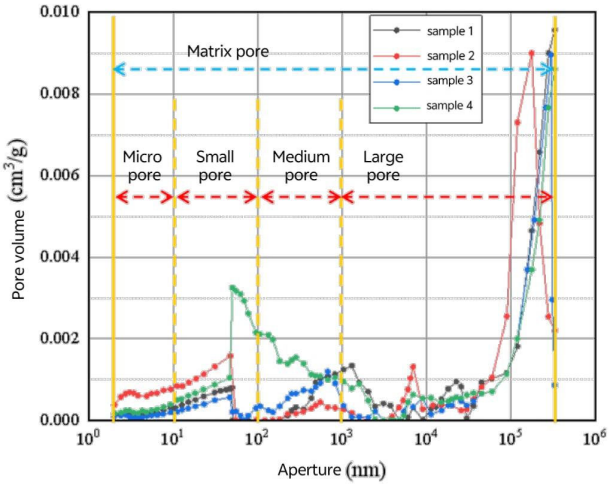

Figure 15. Full aperture distribution curve of Yijianfang Formation in Yueman Block.

(4) Micro reservoir space types in the study area

Through casting thin sections and scanning electron microscopy (Figure 16), it is found that the types of reservoir space in the study area are complex and diverse, including intergranular dissolved pores and intragranular dissolved pores controlled by fabric, as well as pressure-dissolved fractures, shrinkage fractures, and structural fractures not controlled by fabric. Affected by the compaction during the diagenetic process, the reservoir rocks

are dense, the primary pores are not developed, mainly intragranular dissolved pores, and a small amount of intergranular dissolved pores are developed. Affected by compaction and dissolution, structural fractures and pressure solution fractures are developed in the reservoir, and shrinkage fractures are locally visible, some of which are filled with calcite and organic matter. The microscopic reservoir space of Yijianfang Formation in the study area is mainly intragranular dissolved pores, structural fractures, and pressure solution fractures.

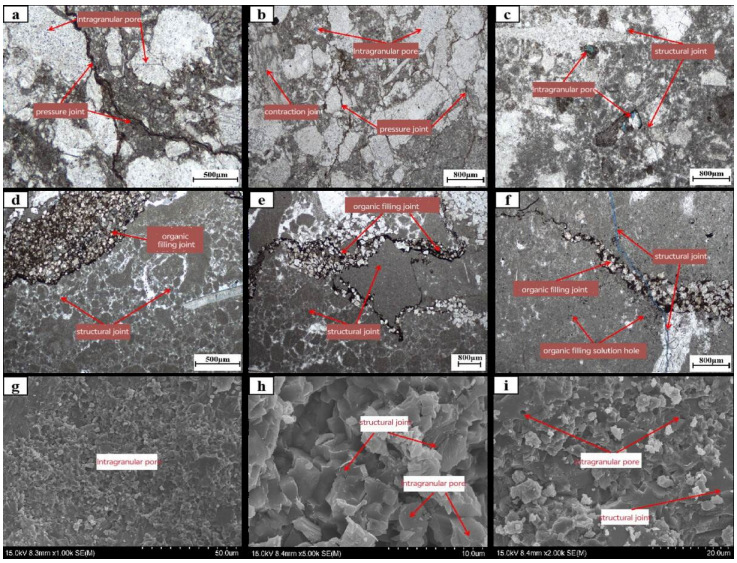

Figure 16. Micro-reservoir space types of Yijianfang Formation in Yueman Block: (**a**) intergranular dissolution pores and pressure dissolution. (**b**) intragranular dissolution pores and pressure dissolution. (**c**) structural fractures and dissolution pores. (**d**) intragranular dissolution and organic matter filling. (**e**) intragranular dissolution pores and cementation. (**f**) intragranular dissolution and structural fractures. (**g**) scanning electron microscopy (sem) image of pore structure. (**h**) shrinkage seams and structural fractures. (**i**) crystalline structures and pore development.

4.2.2. Macroscopic Reservoir Space Characteristics

The fracture-cavity carbonate reservoir of Yijianfang Formation in Yueman Block has developed caves, pores, and fractures, and the reservoir space has developed from nanometer to meter. Through core observation, drilling and logging data, and imaging logging data, the macroscopic reservoir space of the reservoir in the study area is studied.

(1) Cavern

Large caverns are the main reservoir space of fractured-vuggy carbonate reservoir fluid in Yijianfang Formation of Yueman Block. The logging response is characterized by an abnormal increase in well diameter, a sharp decrease in density and acoustic wave value, a significant increase in neutron count, lateral asymmetry in both depth and width, and a marked discrepancy in the microball values, which are notably low, and dark layer on the electrical logging imaging diagram (Figure 17). When encountering caverns in the drilling process, abnormal phenomena such as emptying, mud leakage, and well kick will occur. In the drilling process of Yueman Block, there are 20 wells with emptying, and some emptying wells are shown in Table 4, of which the maximum emptying length is 19.1 m.

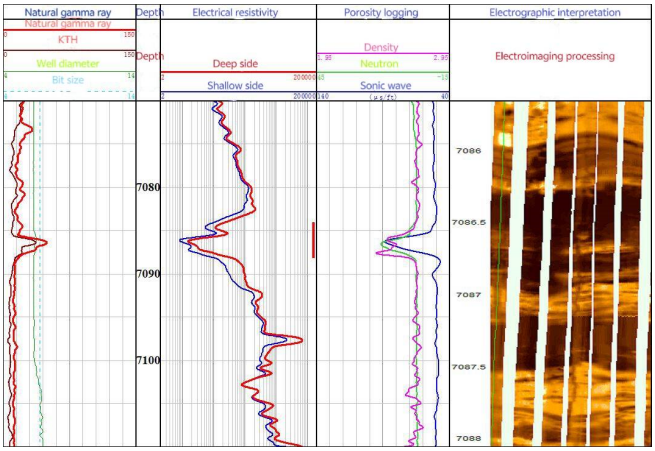

Figure 17. Imaging logging map of cavernous reservoir in Fuman Oilfield (from Tarim Oilfield).

Table 4. Statistical table of partial drilling tool emptying in one room group of Yueman Block.

Well Number	Formation	Depth/m	Emptying/m
M2-4X	Yijianfang Formation	7349.63~7351.04	1.41
M5-4X	Yijianfang Formation	7408.39~7412.54 7412.76~7415	6.39
M5-5	Yijianfang Formation	7259.09~7260.94	1.85
M5-3	Yijianfang Formation	7287.05~7287.94	0.89
M1-3	Yijianfang Formation	7294.14~7295.80	1.66
M3-1	Yijianfang Formation	7246.60~7248.09	1.49
M3-6X	Yijianfang Formation	7399.97~7400.93	0.96
M703	Yijianfang Formation	7300.45~7303.17	2.72
M8-1	Yijianfang Formation	7248.46~7254.80	6.34

(2) Pore

The dissolution pores of Yijianfang Formation in Yueman Block are relatively developed, being honeycomb dissolution pores on the core (Figure 18). The pore-type reservoir shows irregularly distributed dark spots on the electrical imaging logging (Figure 19).

(3) Micro-dislocations

The crack is not only the reservoir space, but also the main channel for fluid migration. Fractures are well developed in Yijianfang Formation in Yueman Block. High-angle fractures, micro-fractures, and sutures can be observed in drilling cores (Figure 20). In the imaging logging, we can observe structural fractures and karst fractures with dark or dark gray sine curves and high-angle lines, as shown in Figure 21.

Figure 18. Core pore photo of Yijianfang Formation, Yueman Block (from Tarim Oilfield).

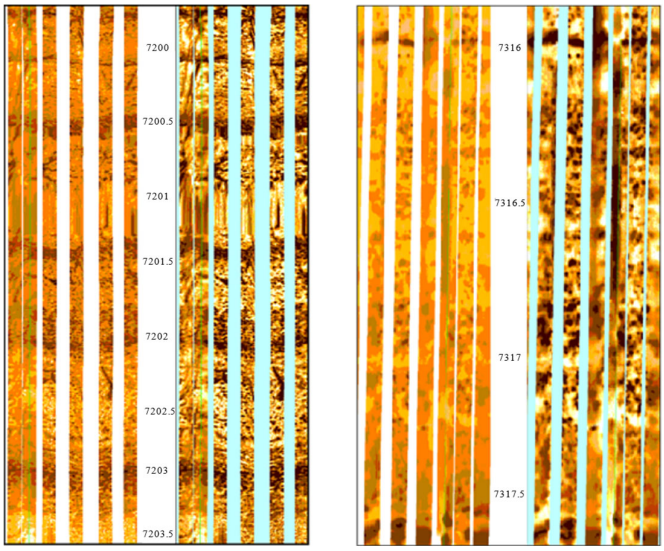

Figure 19. Imaging logging map of hole-type reservoir in Yijianfang Formation, Yueman Block (from Tarim Oilfield).

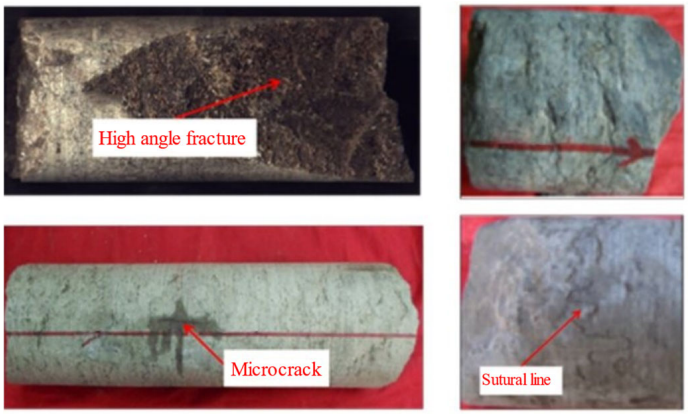

Figure 20. Core fracture photo of Yijianfang Formation, Yueman Block (from Tarim Oilfield).

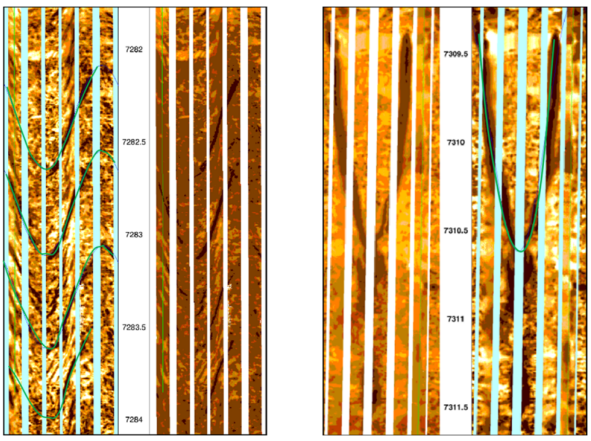

(**a**) (**b**)

Figure 21. Imaging logging map of fractured reservoir in Yijianfang Formation, Yueman Block (from Tarim Oilfield): (**a**) tectonic crack, (**b**) karst crack.

5. Conclusions

(1) The strata of Yueman Block in Fuman Oilfield of Tarim Basin are well developed, and large-scale marine carbonate rocks are developed in Yijianfang Formation of Ordovician, which was the main exploration and development horizon. The overlying Tumuxiuke Formation and Sangtamu Formation have developed thick mudstones, which are high-quality caprocks in this area. Yijianfang Formation has developed multiple sets of strike-slip faults, communicating the deep Lower Cambrian source rocks and playing a good role in dredging.

(2) The lithology of Yijianfang Formation in the Yueman area is mainly micrite and sparry grain limestone. The mineral composition is mainly calcite, containing a small amount of quartz and dolomite.

(3) From the microscopic point of view, the pore size distribution of Yijianfang Formation in Yueman Block is wide, and the pores from nanometer to micron are developed. The primary pores are not developed, mainly including dissolution pores, structural fractures, and pressure-dissolving fractures. The types of reservoir space are mainly divided into caves, cracks, holes, micro-pores, and micro-cracks.

(4) From a macro point of view, drilling and imaging logging data show that the dissolution caves in the study area are developed. According to drilling coring and imaging logging, honeycomb dissolution holes, structural fractures, and karst fractures are developed. The reservoirs of Yijianfang Formation in the study area are mainly cave-type, hole-type, fracture-hole-type, and fracture-type reservoirs. There is a coupling development relationship between fractures and holes, and they are combined to form fracture-cavity bodies with different configurations.

Author Contributions: Conceptualization, C.S. and M.W.; Methodology, Y.Z., L.R., J.L. and X.Z.; Resources, C.L.; Writing—original draft, J.L., X.Z. and M.W.; Writing—review & editing, Y.Z., C.L., L.R. and C.S. All authors have read and agreed to the published version of the manuscript.

Funding: This work was financially supported by the National Natural Science Foundation of China (No. 42472195 and 42272153), the Research Fund of PetroChina Tarim Oilfield Company (No. 671023060003), and the Research Fund of China National Petroleum Corporation Limited (No. 2023ZZ16YJ04).

Data Availability Statement: The original contributions presented in this study are included in the article. Further inquiries can be directed to the corresponding author.

Acknowledgments: The authors received funding from the National Natural Science Foundation of China, the Research Fund of PetroChina Tarim Oilfield Company, and the Research Fund of China National Petroleum Corporation Limited. We gratefully acknowledge these contributions.

Conflicts of Interest: Authors Yintao Zhang and Chong Sun were employed by the company CNPC. The remaining authors declare that the research was conducted in the absence of any commercial or financial relationships that could be construed as a potential conflict of interest.

References

1. Guo, X.; Hu, D.; Huang, R.; Wei, Z. Deep and ultra-deep natural gas exploration in the Sichuan Basin: Progress and prospect. *Nat. Gas Ind. B* **2020**, *7*, 419–432. [CrossRef]
2. He, Z.; Ma, Y.; Zhu, D.; Duan, T.; Gao, Z. Theoretical and technological progress and research direction of deep and ultra-deep carbonate reservoirs. *Oil Gas Geol.* **2021**, *42*, 533–546. [CrossRef]
3. Lai, Q.; Lin, Q.; Chen, S.; Ma, S.; Zhou, Y.; Fang, P.; Yu, R.; Li, S.; Huang, J.; Zheng, J. Resercoir space characteristics and pore structure of Jurassic Lianggaoshan Formation lacustrine shale reservoir in Sichuan Basin, China: Insights into controlling factors. *Front. Earth Sci.* **2023**, *11*, 1133413. [CrossRef]
4. Li, J.; Zhou, H.; Yang, F.; Yang, F.; Liu, S. Research on microscopic characteristics of carbonate reservoir fracture fillings based on microscopic infrared spectroscopy. *Mater. Sci. Eng.* **2016**, *61*, 05013. [CrossRef]
5. Wang, H.; Wang, R.; Zhang, Y.; Li, J.; Wu, Z.; Sun, C.; Liu, Y. Multi-mode flow simulation of fracture-cavity reservoirs and predicting oil accumulation based on hydro-mechanical-damage coupling model. *Geomech. Energy Environ.* **2024**, *38*, 100566. [CrossRef]
6. Zheng, L.; Wang, C.; Jiang, Z.; Wu, Y.; Kong, X.; Zhu, X.; Zhang, Y. Classification and reservoir characteristics of lacustrine carbonate conglomerate in the Shulu Sag of the Bohai Bay Basin. *Mar. Pet. Geol.* **2024**, *164*, 106806. [CrossRef]
7. Dian, B.A.; Wenge, H.U.; Fei, C.A.; Xiaoping, P.E.; Shixi, L.I.; Lin, P.A.; Xiao, W. Development Characteristics and Main Controlling Factors of Reservoir Space in Northern Yujiang Strike-Slip Fault Zone. *Pet. Geol.* **2024**, *45*, 172–180. [CrossRef]
8. Ren, P. Microfacies and Reservoir Space Characteristics of Carbonate Reservoir of the Ordovician Yingshan Formation in Northern Slope of Tazhong Uplift, Tarim Basin. *Geofluids* **2023**, *2023*, 9160334. [CrossRef]
9. Xiang, P.; Ji, H.; Shi, Y.; Huang, Y.; Sun, Y.; Xu, X. Characteristics, Diagenesis, Controlling Factors and Formation Mechanism of Deep-Burial Ordovician Carbonate Reservoirs in the Yangshuiwu Area, Jizhong Depression, Bohai Bay Basin. *Arab. J. Sci. Eng.* **2023**, *48*, 645–663. [CrossRef]
10. Pan, J.; Guo, X.; Gu, T.; Yang, S.; Yang, R.; Gong, H. Characterization of Carbonate Reservoirs and Main Controlling Factors Research. *Chem. Technol. Fuels Oils* **2024**, *60*, 897–909. [CrossRef]
11. Huang, W.; Wang, A.; Wan, H. Discussion on characteristics of the Cambrian-Ordovician carbonate rocks reservoirs and origin of dolostones in Tarim Basin. *J. Palaeogeogr.* **2012**, *6*, 288–293. [CrossRef]
12. Jiang, Z.; Zhang, W.; Liang, C.; Wang, Y.; Liu, H.; Chen, X. Basic characteristics and evaluation of shale oil reservoirs. *Pet. Res.* **2016**, *1*, 149–163. [CrossRef]
13. Ding, X.; Liu, X.; Qi, Z.; Zhang, W.; Liu, S. Reservoir space characterization of vuggy carbonate reservoirs with multiple scales: A case study of Ma 5-7 interval, Middle Ordovician Majiagou Formation, Daniudi area, Ordos Basin. *Pet. Geol. Exp.* **2021**, *43*, 689–696. [CrossRef]
14. Lu, X.; Min, Z.; Hu, X.; Jin, Y. Studies of 3D reservoir modeling:taking Ordovician carbonate fractured-vuggy reservoirs in Tahe Oil Field as an example. *Pet. Geol. Exp.* **2012**, *34*, 193–198.
15. Jiang, T.; Deng, X.; Cao, P.; Chang, S. Storage space types and water-flooding efficiency for fault-controlled fractured oil reservoirs in Fuman oilfield, Tarim Basin. *Oil Gas Geol.* **2024**, *45*, 542–552.
16. Fu, S.; Fu, J.; Niu, X.; Li, S.; Wu, Z.; Zhou, X.; Liu, J. Reservoir formation conditions and key technologies for exploration and development in Qingcheng large oilfield. *Pet. Res.* **2020**, *5*, 181–201. [CrossRef]
17. Shen, W.; Chen, F.; Wang, Y.; Zhang, K.; Chen, Z.; Luo, G.; Fu, X. The origin migration and accumulation of the Ordovician gas in the Tazhong III region, Tarim Basin, NW China. *Mar. Pet. Geol.* **2019**, *101*, 55–57. [CrossRef]
18. Zhu, G.; Milkov, A.V.; Li, J.; Xue, N.; Chen, Z. Deepest oil in Asia: Characteristics of petroleum system in the Tarim basin, China. *J. Pet. Sci. Eng.* **2021**, *199*, 108246. [CrossRef]
19. Zhao, H.; Li, B.; Zhou, Y.; Zhang, Q.; Liu, H.; Wang, W.; Wang, X. A connectivity prediction model for fault-karst reservoirs based on high-speed non-Darcy flow. *Acta Pet. Sin.* **2022**, *43*, 1026–1034. [CrossRef]
20. Han, Y.; Zhang, Y.; Chen, W. Geological conditions and evolution for the accumulation of the ultra-deep oil pools in the Yueman area, Tarim Basin. *Nat. Gas Geosci.* **2021**, *32*, 1634–1645. [CrossRef]
21. Wu, C.; Zhao, X.; Wu, G.; Li, F.; Zhang, H.; Hu, Z.; Li, S. Characteristics and distribution of fault−controlled carbonate reservoirs in Yijianfang Formation of Yueman area, northern Tarim Basin. *Geol. China* **2024**, *51*, 762–779. [CrossRef]

22. Wu, G.; Ma, B.; Han, J.; Guan, B. Origin and growth mechanisms of strike-slip faults in the central Tarim cratonic basin, NW China. *Pet. Explor. Dev.* **2021**, *48*, 595–607. [CrossRef]
23. Yao, Y.; Zeng, L.; Mao, Z.; Han, J.; Cao, D.; Lin, B. Differential deformation of a strike-slip fault in the Paleozoic carbonate reservoirs of the Tarim Basin, China. *J. Struct. Geol.* **2023**, *173*, 104908. [CrossRef]
24. Zhang, H.; Cai, Z.; Qi, L.; Yun, L.; Tang, P.; He, J. Stratigraphic recognition and correlation of Middle Ordovician Yijianfang Formation in northwestern Tazhong uplift and its geological significances. *Acta Pet. Sin.* **2017**, *38*, 622–635.
25. Liu, J.; Chen, Q.; Wang, P.; You, D.; Xi, B.; Gong, H. Characteristics and main controlling factors of carbonate reservoirs of Middle-Lower Ordovician, Shunnan area, Tarim Basin. *Pet. Geol. Exp.* **2021**, *43*, 23–33. [CrossRef]
26. Ning, F.; Yun, J.; Zhang, Z.; Li, P. Deformation patterns and hydrocarbon potential related to intracratonic strike-slip fault systems in the east of Central Uplift Belt in the Tarim Basin. *Energy Geosci.* **2022**, *3*, 63–72. [CrossRef]
27. Lu, Z.; Ping, H.; Chen, H.; Zhang, Y.; Xie, Z.; Zhang, Y.; Chen, Z.; Zhang, X.; Yang, K.; Li, X. Geochemical characteristics of Ordovician crude oils in the F_I17 strike-slip fault zone of the Fuman oilfield, Tarim basin: Implications for ultra-deep hydrocarbon accumulation in the Tarim basin. *Mar. Pet. Geol.* **2024**, *163*, 106800. [CrossRef]
28. Hu, X.; Zheng, W.; Zhao, X.; Niu, B. Quantitative characterization of deep fault-karst carbonate reservoirs: A case study of the Yuejin block in the Tahe oilfield. *Energy Geosci.* **2023**, *4*, 100153. [CrossRef]
29. Wei, J.; Zhou, X.; Shamil, S.; Yuriy, K.; Yang, E.; Yang, Y.; Wang, A. High-pressure mercury intrusion analysis of pore structure in typical lithofacies shale. *Energy* **2024**, *295*, 130879. [CrossRef]
30. Li, J.; Kong, X.; Song, M.; Wang, Y.; Wang, X.; Liu, X.L. Study on the influence of reservoir rock micro-pore structure on rock mechanical properties and crack propagation. *Rock Soil Mech.* **2019**, *40*, 4149–4156. [CrossRef]
31. Liu, Q.; Cai, Z.; Xue, Y. Full pore size characterization of dolomite pore structure of Xiaolbulake Formation in the Peripheral Area of Keping, Tarim Basin. *Sci. Technol. Eng.* **2022**, *22*, 5213–5221.
32. Zhu, G.; Xie, Z.; Wang, T. Microscopic pore structure characteristics of Shanxi Formation coal reservoir in Daning-Jixian Block. *Saf. Coal Mines* **2024**, *55*, 31–42.
33. Yin, J.; Hu, P.; Guo, Y.; Li, Y.; Luo, S. Petrological Characteristics and Hydrocarbon Generation of Carbonate Source Rocks of the Permian Taiyuan Formation in Central and Eastern Ordos Basin, China. *Minerals* **2023**, *13*, 1058. [CrossRef]
34. Zhou, X.; Guo, W.; Li, X.; Liang, P.; Yu, J.; Zhang, C. Deciphering Nano-Resolution Petrological Characteristics of the Siliceous Shale at the Bottom of the Longmaxi Formation in the Zigong Area, Sichuan Basin, China: Deep-Water Microbialites. *Minerals* **2024**, *14*, 1020. [CrossRef]
35. Cao, Y.; Chen, J.; Han, W.; Li, Z.; Huang, H.; Suo, G. The Influence Law and Mechanism of CO2 Injection Pressure on Coal Rock Pore-Fracture Characteristics. *Chem. Technol. Fuels Oils* **2023**, *59*, 638–646. [CrossRef]
36. Qi, L.; Tang, X.; Wang, Z.; Peng, X. Pore characterization of different types of coal from coal and gas outburst disaster sites using low temperature nitrogen adsorption approach. *Int. J. Min. Sci. Technol.* **2017**, *27*, 371–377. [CrossRef]
37. Zhang, B.; Chen, Y. Particle size effect on pore structure characteristics of lignite determined via low-temperature nitrogen adsorption. *J. Nat. Gas Sci. Eng.* **2020**, *84*, 103633. [CrossRef]